Journal of Physics D:
Applied Physics

Optimize wet etch method for high yield AlAsSb/ InGaAs avalanche photodiode fabrication

To cite this article before publication: Haifeng Kan *et al* 2026 *J. Phys. D: Appl. Phys.* in press https://doi.org/10.1088/1361-6463/ae357a

IOP Publishing Journal Title
Journal **XX** (XXXX) XXXXXX https://doi.org/XXXX/XXXX

Optimize wet etch method for high yield AlAsSb/ InGaAs avalanche photodiode fabrication

Haifeng Kan[1,†], Danqi Lei[1,†,*], Xuanchang Zhang[1], Hexing Wang[1], Suguo Huo[2], Baolai Liang[3], Huiyun Liu[1], Mingchu Tang[1]

[1] Department of Electronic and Electrical Engineering, University College London, Torrington Place, London WC1E 7JE, United Kingdom

[2]London Centre for Nanotechnology, 17-19 Gordon Street, London, WC1H 0AH, United Kingdom

[3]Department of Electrical and Computer Engineering, California NanoSystem Institute, University of California - Los Angeles, Los Angeles, CA 90095, USA

†These authors contributed equally to this work.

E-mail: danqi.lei@ucl.ac.uk

Received xxxxxx
Accepted for publication xxxxxx
Published xxxxxx

Abstract

The AlAsSb avalanche photodiode is a type of excellent high-sensitivity infrared detectors with low excess noise, owing to the intrinsic low β to α ratio of AlAsSb. This material overcomes the challenge of achieving low noise performance in conventional InP-based infrared avalanche photodiodes. However, from a fabrication perspective, AlAsSb gets oxidized rapidly during the etching process, which significantly hinders device properties, therefore, reduces device yield. In this work, we optimize a wet etching method utilizing a mixture of H_2SO_4:H_2O_2: H_2O for etching non-Sb contained layers, followed by a mixture of HCl: H_2O_2: H_2O for etching Sb-contained layers. A summary of etching rates for different etching solution combinations is illustrated. Here firstly proposes to deploy an oxidization induced colour changing as an indicator to swap etching solution. This method has been examined and supported by EDX results and SEM images. A comparison between two avalanche photodiodes with and without residues confirms that the dark current of the avalanche photodiode is reduced two orders of magnitude with clean surface.

Keywords: APD, AlAsSb material, wet etching method

1. Introduction

Low-noise, high-sensitivity avalanche photodiodes (APDs) operating at 1550 nm are essential for applications such as fibre-optic communication, eye-safe LiDAR, and infrared imaging [1-4]. Conventional InAlAs/InP based APDs, although widely adopted, suffer from excess avalanche noise due to their nearly symmetric electron and hole ionisation coefficients (e.g. $\beta/\alpha \approx 0.6–0.9$). This symmetry limits the gain-bandwidth product (GBP) and degrades signal-to-noise ratio under high-speed or low-light operating conditions [5, 6].

Recent studies have shown that $AlAs_{0.56}Sb_{0.44}$ and $Al_xGa_{1-x}As_{0.56}Sb_{0.44}$, a III-V compound lattice-matched to InP, exhibits highly asymmetric ionisation behaviour with β/α ratios as low as 0.005 ($k \approx 0.005$) [7-9]. These characteristics lead to extremely low excess noise factor which belows 1.5 at gain values of M = 30, even for PIN structures with avalanche layer thicknesses up to 1.55 μm [7, 10, 11]. Moreover, excess

noise in $Al_xGa_{1-x}AsSb$ alloys, showing ultralow noise in high-Al compositions (F<2 up to M≈60–90) and increasing noise as Al content decreases [12]. In contrast to InAlAs, which typically requires very thin multiplication layers to suppress noise, Sb digital alloy enables both high gain and low excess noise in thicker devices [11, 13-16]. Numerical modelling predicts that InGaAs/AlAsSb SAM-APDs with multiplication regions between 600 nm and 1500 nm can achieve receiver sensitivity down to −25.7 dBm at 25 Gb/s with BER = 10^{-12} and responsivity of 0.92 A/W [7].

Although AlAsSb demonstrates excellent avalanche behaviour and low noise, its strong oxidation tendency prevents high yield fabrication [17]. The oxidation residues on the sidewall or contact layers can lead to surface leakage and breakdown voltage instability, particularly in mesa-type APD structures [7]. Both wet etching and dry etching processes struggle to fully remove the AlAsSb oxidized residues. In particular, dry etching methods based on Cl_2/N_2 plasma have been shown to cause surface damage, such as rough sidewalls and profile distortion, especially under high RF power or elevated temperatures [18]. While a wet etching method has been developed for GaSb grown on GaAs substrates, a detailed wet etching process for AlAsSb on InP wafers has not yet been reported [19].

In this work, we investigate wet chemical treatment strategies aimed at removing resdues generated during the AlAsSb etching process. This is the first, from the author's knowledge, reports the oxidized AlAsSb material color changing corresponding to oxidized material distribution. Specifically, we identify an optimized two-step wet etching method by analysing surface roughness, chemical composition of residues, and etching duration.We also compare the dark current and voltage characteristics of devices with and without oxidized AlAsSb residues.

2. Device Structure

InGaAs/AlAsSb heterostructure diodes wafer was grown on an InP semi-insulating (SI) substrate using molecular-beam epitaxy (MBE). The layer structure is illustrated in Fig. 1(a). A 500 nm $InGa_{0.54}As$ layer with a heavy doping concentration of 1 x 10^{19} cm^{-3} was first grown on the InP substrate to serve as the n-contact layer. This was followed by a 100 nm n-type doped AlAsSb cladding layer and a 600 nm undoped AlAsSb multiplication layer. An 80 nm AlAsSb charge layer was inserted to modulate the electric field distribution, preceding a 500 nm InGaAs absorption layer. Finally, p-type cladding and contact layers were grown, with doping concentrations of 2 × 10^{18} cm^{-3} and 1 × 10^{19} cm^{-3}, respectively. Fig.(b) and (c) illustrate the top view and cross-section diagram of the designed APD which is passivated by SU-8.

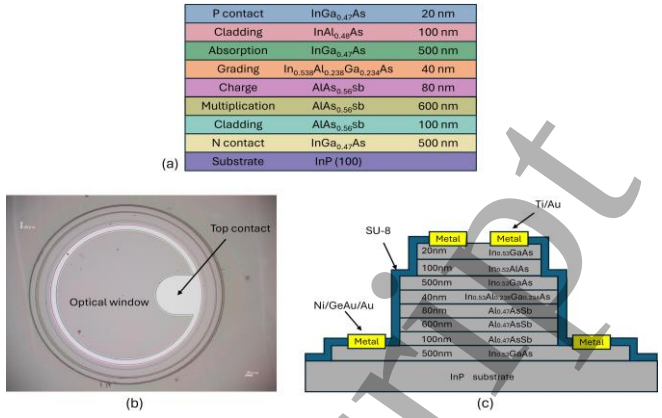

Fig.1.(a) Layer structure of the designed diode heterostructure based on a semi-insulating (SI) InP substrate; (b) Top view of the designed AlAsSb/InGaAs/InP APD (c) The cross-sectional diagram of the designed APD.

The energy band diagram of the AlAsSb/InGaAs/InP backward diode is shown in Fig. 2. The structure is terminated by p-type and n-type InGaAs layers on both sides. A 500 nm undoped InGaAs layer, located beneath the InAlAs cladding, serves as the separate absorption layer. A highly p-doped AlAsSb charge layer is inserted adjacent to the InAlGaAs barrier to modulate the backward current relative to the forward current as illustrated in Fig. 2. The Fermi level in the InGaAs and AlAsSb layers lie close to or above the valence band edge, allowing electrons from the AlAsSb valence band to tunnel freely into the InGaAs conduction band. This band structure asymmetry results in a backward current significantly greater than the forward current.

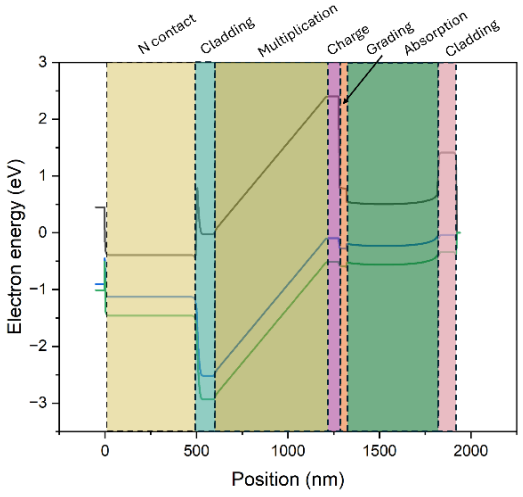

Fig. 2. Modeled energy band diagram at zero bias.

3. Method

A typical separate absorption and multiplication (SAM) avalanche photodiode performs a higher gain and a large gain

bandwidth by deploying different materials in absorption and multiplication layers. A 500 nm InGaAs undoped layer and a 600 nm undoped AlAsSb serve as absorption and multiplication layer separately due to their different bandgap and ionisation coefficient [20]. However, the InGaAs and AlAsSb are difficult to be etched effectively and smoothly, even by utilising versatile acid combination of citric acid and phosphoric acid [21]. A non-selective etchant yields a very low etch rate of approximately 1 nm/ min under 4 °C, making it impractical for device thicker than 1 µm [22]. A two-step etching approach which previously applied in low excess and high gain AlAsSb APD fabrications [10, 14] has been optimized in this work. The process uses a H_2SO_4:H_2O_2: H_2O mixture to etch InGaAs and InAlAs, followed by a HCl: H_2O_2: H_2O solution for the AlAsSb layer. Here we observe that the endpoint of etching can be clearly identified by a colour change. Surface roughness and chemical residue composition were examined in detail.

Fig. 3 illustrates the surface conditions of the APD material by applying test patterns with stripe shape to clarify the surface changes during the two-step etching process. In the first step, the InGaAs and InAlAs layers were etched using H_2SO_4:H_2O_2:H_2O, followed by etching of the AlAsSb layer using HCl: H_2O_2: H_2O. Microscope and atomic force microscopy (AFM) images were used to assess the surface. Fig. 3(a) shows the oxidized AlAsSb surface after completion of the first etching step. The surface turns black when the etchant reaches the AlAsSb layer. It indicates to change solution to etch the oxidized AlAsSb by HCl:H_2O_2:H_2O (1:1:3) for 5 seconds resulting in a smooth and clean surface, as shown in Fig. 3(b). AFM analysis was conducted over a 1 µm² area. The images in Fig. 3(c) and 3(d) correspond to etching with H_2SO_4:H_2O_2:H_2O (1:10:80) and HCl:H_2O_2:H_2O (1:1:3), respectively. The surface in Fig. 3(c) exhibits a roughness of approximately 150 nm, which is roughly three times greater than that in Fig. 3(d). This implies that the HCl:H_2O_2:H_2O solution effectively removes the oxidized AlAsSb layer. To further understand the dark residues remaining after the first etch, we analysed SEM and EDX images of the affected surface.

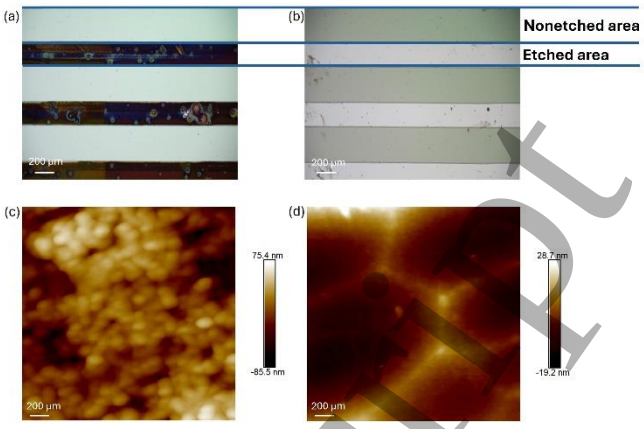

Fig. 3. (a) Microscope image of test stripe pattern, showing AlAsSb after H_2SO_4: H_2O_2: H_2O etched off top InGaAs layer. (b) Image of bottom InGaAs layer after AlAsSb residual removed by HCl: H_2O_2: H_2O solution. (c) AFM image of 1 µm² area of AlAsSb material after etching with H_2SO_4: H_2O_2: H_2O (d) AFM image of 1 µm² area of AlAsSb material after etching with HCl: H_2O_2: H_2O solution.

AlAsSb Etching

To investigate the oxidized AlAsSb layer, we examined the material cross-section using a scanning electron microscope (SEM). Fig. 4(a) shows the cross-section of the oxidized AlAsSb surface, where a clear detachment between layers was observed. Once oxidized, the AlAsSb layer separated from the underlying InGaAs layer, making it difficult to determine the etching depth by simply measuring the sample thickness. Such cracking is caused by Sb oxidization. The strain generated by the lattice constant variation of oxidized AlAsSb layer introduces a lattice and a material delamination from InGaAs underneath leading to a crack shown in Fig.4(a). It was also challenging to assess the etch rate based on the surface profile. Fig. 4(b) shows the cross-section after the AlAsSb layer was removed using the HCl:H_2O_2:H_2O solution. An undercut of approximately 1.5 µm remained at the sidewall after the second etching step. This undercut will later be filled using SU-8 passivation during APD device fabrication.

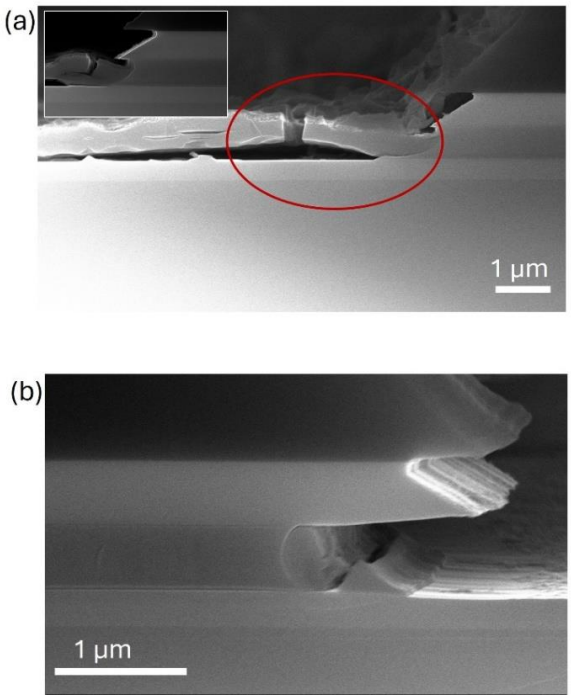

Fig. 4. (a) A SEM image of the oxidized AlAsSb layer cross-section. The inset is the magnified image of the etching boundary. (b) A SEM image of AlAsSb/InGaAs wafer after oxidized AlAsSb etched off by HCl: H_2O_2: H_2O solution.

This material delamination inhibits to inspect the etching depth of the AlAsSb layer precisely. However, we have observed the colour changing during etching this layer. To further study the chemical composition of the (delaminate dark material) oxidized residues, we selected an area that contains oxidized and unoxidized AlAsSb material shown in Fig. 5. An element distribution of EDX (Energy dispersive X-ray) spectroscopy image is illustrated in Fig. 5(a). The corresponding SEM image of this area is shown in Fig. 5(b). The distribution of elements, including In, Ga, As, Sb, O, Al, have been presented in Fig. 5(a). Corresponding to the inspected region in Fig. 5(b), In, Ga, As (indicated as InGaAs layer) distributes at mask area and where the oxidized AlAsSb peeled off. It is worth noting that oxidized area where O element distributes fully broke into pieces. The non-oxidized area is still flat. It indicates that the surface becomes rougher once the AlAsSb layer is oxidized. It is difficult to inspect the etching rate during the AlAsSb etching process. However, the distinct colour changing sends the signal at an etching terminated point. Fig. 5(c) and (d) presents the microscope image and SEM image of the same oxidized AlAsSb area. The black and cracked area indicates the oxidized area while the white area where surface is flat and intact is the non-oxidized AlAsSb area. It implies that the colour changing can be considered as a remarkable sign of oxidation. It is reliable to inspect the colour as a turning point to swap the solution from H_2SO_4: H_2O_2: H_2O to HCl: H_2O_2: H_2O.

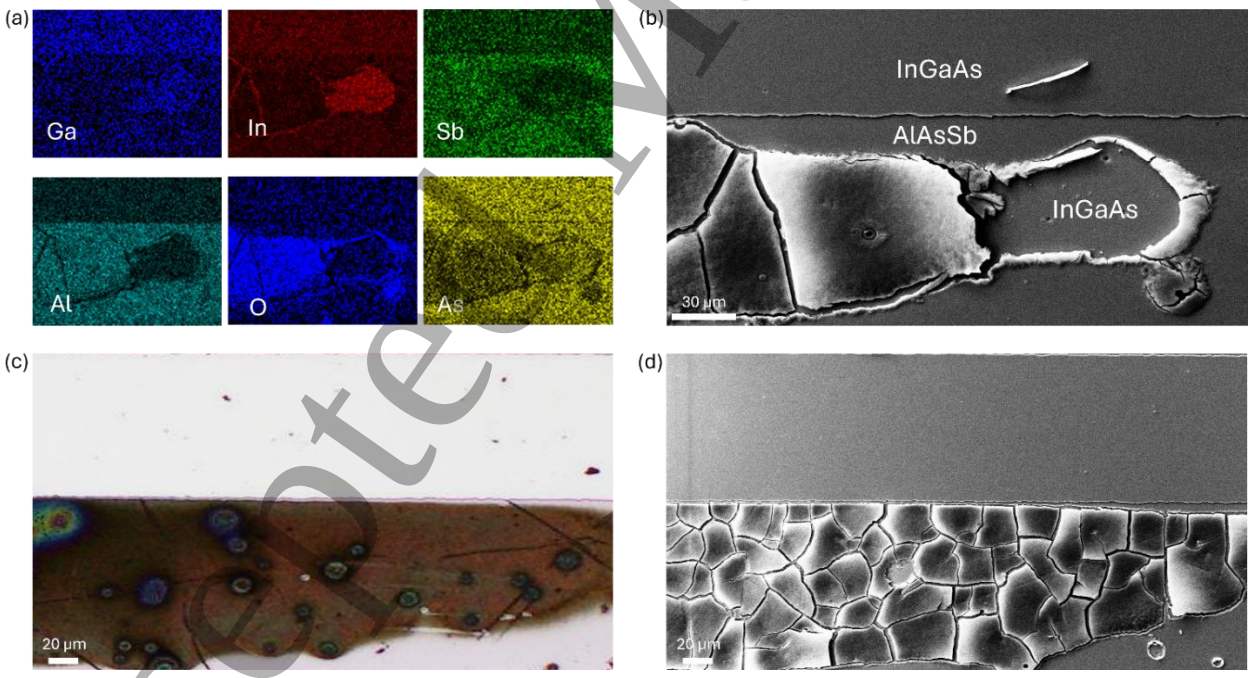

Fig. 5. (a) Elements distribution of EDX (Energy dispersive X-ray) spectroscopy image of AlAsSb residues on an etching surface (b) A SEM image corresponding to EDX examining area. (c) Microscope image of oxidized AlAsSb area. (d) A SEM image corresponding to the Microscope image.

Furthermore, the etching performance of H_2SO_4: H_2O_2: H_2O (1:10:80) is also when applied solely to the AlAsSb layer. As shown in Fig. 6(a), this solution partially removed the residues but failed to fully clean the surface. According to the device structure shown in Fig .1(b) and (c), the residuals left on the n-doped InGaAs layer prohibits a uniform n-contact being formed. In contrast, the HCl:H_2O_2:H_2O (1:1:5) solution successfully etched the entire AlAsSb layer and produced a clean surface, as shown in Fig. 6(b). While the H_2SO_4:H_2O_2:H_2O solution achieves a smoother surface to InGaAs layer with an etch rate of approximately 12 nm/s. Therefore, it is essential to alternate etchants depending on whether the target layer contains antimony.

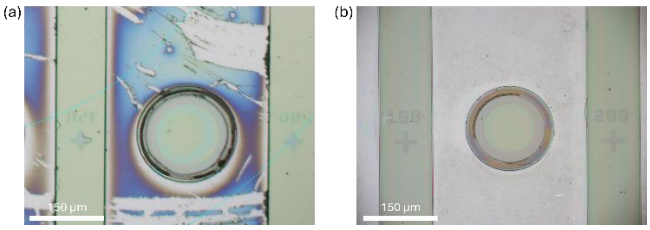

Fig. 6. (a) The microscope images of the AlAsSb layer etched by H_2SO_4: H_2O_2: H_2O (1:10:80); (b) The microscope image of the AlAsSb layer etched by HCl:H_2O_2:H_2O (1:1:5).

Table 1 summarises the etch rates of AlAsSb using different HCl:H_2O_2:H_2O ratios. The etch rate decreases from 129 nm/s for a 1:1:3 mixture to 20 nm/s for a 1:1:6 ratio. However, the actual etch rate is highly sensitive to air exposure during the process. The values reported here were measured from a single uninterrupted etching step conducted without exposing the sample to air.

Table 1. Etching rates of AlAsSb using various HCl: H_2O_2: H_2O mixtures. Measurements were conducted in a single continuous process without air exposure.

HCl: H_2O_2 : H_2O	Etching Rate (nm/s)	Etch Time (s)
1:1:3	129	5
1:1:4	40	16
1:1:5	25	25
1:1:6	20	32

4. Dark Current and Gain of AlAsSb Devices

We compared the dark current and voltage characteristics of devices with and without oxidized AlAsSb residues. As shown in Fig. 7(a), the dark current of the APD was reduced by up to two orders of magnitude. The 150 µm diameter device without surface residues exhibited a dark current one to two orders of magnitude lower than that of the device with oxidized residues. The dark current of this AlAsSb APD is lower than the AlAsSb APD reported in [23], however, it is slightly larger than AlGaAsSb layer based APD [24].The multiplication factor of the devices shown in Fig.7(b) implies that APD device without residuals demonstrates a higher gain than the device with residuals. The gain is calculated with an extracted photocurrent at a low-bias point (-10 V), following the same approached adopted in other APD devices [10, 25]. A clean surface also enhances the gain of AlAsSb APDs. However, the gain achieve by our device is slightly lower than the device reported in literature [23]. We believe that the thickness of the multiplication layer has to be optimized to achieve higher gain. These results highlight the importance of achieving a clean etched surface in the fabrication of low-dark-current APDs.

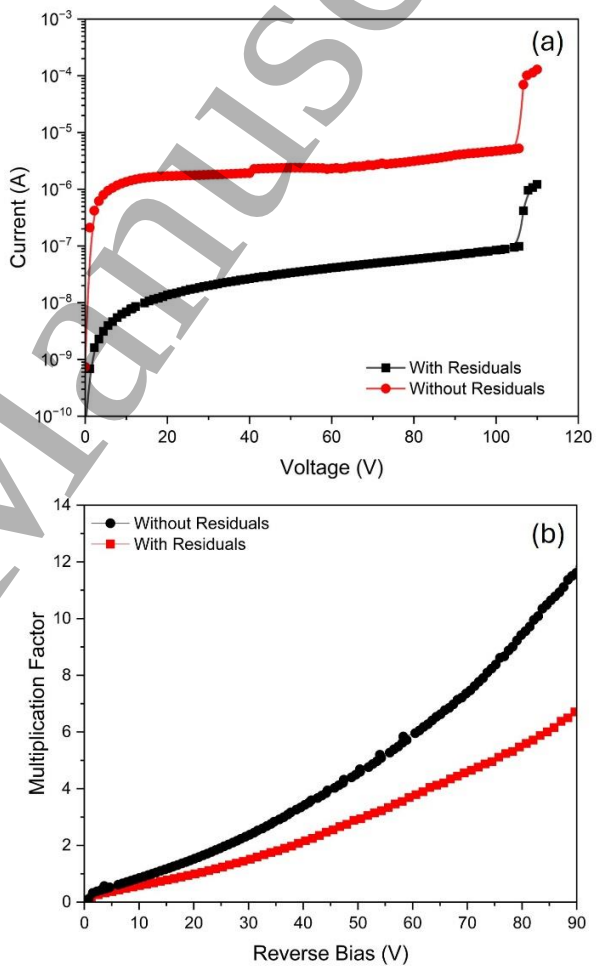

Fig. 7. (a) Dark current of 150 µm diameter device with oxidized AlAsSb residues and without oxidized AlAsSb residues;(b) Measured multiplication factor versus applied reverse bias for device with and without residues.

5. Conclusion

In summary, we have presented an optimized wet etching method based on a specific two-step sequence. This is the first

time a color indicated etching method has been reported for InGaAs/AlAsSb SAM avalanche photodiode. A comprehensive analysis was carried out to investigate the morphology and composition of the oxidized AlAsSb layer. We found that the appearance of a uniformly dark surface is a more reliable indicator of etching completion than depth measurements, due to the surface cracking/delamination caused by oxidation. APD devices fabricated with minimal AlAsSb residues exhibited dark currents approximately one order of magnitude lower than those with significant oxidized residues. These results demonstrate that the proposed wet etching method is both effective and easy to implement, making it highly suitable for high yield APD fabrication.

Acknowledgements

This work was supported by the National Key R&D Program of China (Grant No. 2023YFB2805900, S. C), Engineering and Physical Sciences Research Council (Grant Numbers EP/Z532848/1, EP/X015300/1, EP/T028475/1 and EP/P006973/1) and SPIKEPro which was received funding from the European Union's Horizon 2020 programme under grant agreement number 101129904.

Data Availability

All data that support the findings of this study are included within the article (and any supplementary files).

References

1. Campbell JC, Demiguel S, Ma F, Beck AL, Guo X, Wang S. Recent advances in avalanche photodiodes. IEEE J Sel Top Quantum Electron 2004;10:777–87.
2. Yoshimatsu T, Nada M, Oguma M, Yokoyama H, Ohno T, Doi Y, et al. Compact and high-sensitivity 100-Gb/s (4× 25 Gb/s) APD-ROSA with a LAN-WDM PLC demultiplexer. Opt Express 2012;20:B393–8.
3. Ong DSG, Ng JS, Hayat MM, Sun P, David JPR. Optimization of InP APDs for High-Speed Lightwave Systems. J Lightwave Technol 2009;27:3294–302.
4. Hayashi M, Watanabe I, Nikata T, Makita K, Yamakata S, Taguchi K. Microlens-integrated large-area InAlGaAs-InAlAs superlattice APD's for eye-safety 1.5-µm wavelength optical measurement use. IEEE Photon Technol Lett 1998;10:576–8.
5. Nada M, Yoshimatsu T, Muramoto Y, Yokoyama H, Matsuzaki H. Design and Performance of High-Speed Avalanche Photodiodes for 100-Gb/s Systems, Beyond. J Lightwave Technol 2015;33:984–90.
6. Umebu I, Choudhury ANMM, Robson PN. Ionization coefficients measured in abrupt InP junctions. Appl Phys Lett 1980;36:302–3.
7. Yi X, Xie S, Liang B, Lim WL, Cheong JS, Debnath MC. Extremely low excess noise and high sensitivity $AlAs_{0.56}Sb_{0.44}$ avalanche photodiodes. Nat Photonics 2019;13:683–6.
8. Jin X, Xie S, Liang B, Yi X, Lewis H, Lim LW. Temperature Dependence of the Impact Ionization Coefficients in AlAsSb Lattice Matched to InP. IEEE J Sel Top Quantum Electron 2021;28:1–8.
9. Campbell JC, David JPR, Bank SR. Sb-Based Low-Noise Avalanche Photodiodes. Photonics 2023;10:715.
10. Xie S, Tozer RC, Tan CH. Excess Noise Characteristics of Thin AlAsSb APDs. IEEE Trans Electron Devices 2012;59:1475–9.
11. Rockwell AK, Yuan Y, Jones AH, March SD, Bank SR, Campbell JC. $Al_{0.8}In_{0.2}As_{0.23}Sb_{0.77}$ Avalanche Photodiodes Avalanche Photodiodes. IEEE Photon Technol Lett 2018;30:1048–51.
12. Yi, Xin, Xiao Jin, Baolai Liang, Harry Lewis, Qingyu Tian, Chee H. Tan, Shiyu Xie et al. Excess noise in $Al_xGa1\text{-}xAs_{0.56}Sb_{0.44}$ lattice matched to inp at room temperature. oxical Components and Materials XXII 2025; 146-150.
13. Lee, S., Guo, B., Kodati, S.H., Jung, H., Schwartz, M., Jones, A.H., Winslow, M., Grein, C.H., Ronningen, T.J., Campbell, J.C. and Krishna, S.. Random alloy thick AlGaAsSb avalanche photodiodes on InP substrates. 2022; Applied Physics Letters, 120(7).
14. Lee S, Jin X, Jung H, Lewis H, Liu Y, Guo B, et al. High gain, low noise 1550 nm GaAsSb/AlGaAsSb avalanche photodiodes. Optica 2023;10:147–54.
15. Ren M, Maddox SJ, Woodson ME, Chen Y, Bank SR, Campbell JC. Low excess noise AlxIn1-xAsySb1-y (x;0.3-0.7) avalanche photodiodes. In: Conference on Lasers and Electro-Optics (CLEO); 2016 Jun 5–10; San Jose, CA. Washington: Optical Society of America; 2016. p. 1–2.
16. Ren M, Maddox SJ, Woodson ME, Chen Y, Bank SR, Campbell JC. AlInAsSb separate absorption, charge, and multiplication avalanche photodiodes. Appl Phys Lett 2016;108:191108.
17. Blum O, Hafich MJ, Klem JF, Baucom K, Allerman A. Wet thermal oxidation of AlAsSb against As/Sb ratio. Electron Lett 1997;33:1097–9.
18. Huang M, Chen J, Xu J, Wang F, Xu Z, He L, et al. ICP etching for InAs-based InAs/GaAsSb superlattice long wavelength infrared detectors. Infrared Phys Technol 2018;90:110–14.
19. Dier O, Lin C, Grau M, Amann MC. Selective and non-selective wet-chemical etchants for GaSb-based materials. Semicond Sci Technol 2004;19:1250–53.
20. Xie J, Ng JS, Tan CH. An InGaAs/AlAsSb avalanche photodiode with a small temperature coefficient of breakdown. IEEE Photon J 2013;5:6800706.
21. Liu, B., Zhu, L., Lu, L., Chen, W., Gong, R., Xie, N., Gong, M., Feng, Q., Chen, Y., Zheng, X. and Dong, M.,. MBE growth of mid-wavelength type II InAs/InAsSb superlattice photodetectors with wet etching and Al2O3 passivation. 2024;Vacuum, 224, p.113087.
22. Jönsson A, Xu P, Reitemeier J, Bohn PW, Fay P. Wet etch methods to achieve submicron active area self-aligned vertical Sb-heterostructure backward diodes. Mater Sci Semicond Process 2024;171:108036.

23. Yi X, Xie S, Liang B, Lim LW, Zhou X, Debnath MC, et al. Demonstration of large ionization coefficient ratio in $AlAs_{0.56}Sb_{0.44}$ lattice matched to InP. Sci Rep 2018;8:9107.
24. Jin, X., Lewis, H.I., Yi, X., Xie, S., Liang, B., Huffaker, D.L., Tan, C.H. and David, J.P.. Impact ionization coefficients and excess noise in Al0. 55Ga0. 45As0. 56Sb0. 44 lattice matched to InP. 2024;Applied Physics Letters, 124(25).
25. Qian, L., Zhao, X., Zhang, K., Huo, C., Li, Y., Yan, N., Shi, F., Peng, X. and Chen, M.. Si-HgTe Quantum Dot Visible-Infrared Photodetector. Nanomaterials,2025; 15(4), p.262.